Cancer Cell
Article

Blocking Neuropilin-1 Function Has an Additive Effect with Anti-VEGF to Inhibit Tumor Growth

Qi Pan,[1,7] Yvan Chanthery,[1,7] Wei-Ching Liang,[2] Scott Stawicki,[2] Judy Mak,[1] Nisha Rathore,[3] Raymond K. Tong,[4] Joe Kowalski,[1] Sharon Fong Yee,[5] Glenn Pacheco,[5] Sarajane Ross,[5] Zhiyong Cheng,[1] Jennifer Le Couter,[1] Greg Plowman,[1] Franklin Peale,[3] Alexander W. Koch,[4] Yan Wu,[2,*] Anil Bagri,[1] Marc Tessier-Lavigne,[6] and Ryan J. Watts[1,*]
[1] Tumor Biology and Angiogenesis
[2] Antibody Engineering
[3] Pathology
[4] Protein Chemistry
[5] Translational Oncology
[6] Research Drug Discovery
Genentech, Inc., 1 DNA Way, South San Francisco, CA 94080, USA
[7] These authors contributed equally to this work.
*Correspondence: rwatts@gene.com (R.J.W.), yw@gene.com (Y.W.)
DOI 10.1016/j.ccr.2006.10.018

SUMMARY

Neuropilin-1 (NRP1) guides the development of the nervous and vascular systems. Binding to either semaphorins or VEGF, NRP1 acts with plexins to regulate neuronal guidance, or with VEGFR2 to mediate vascular development. We have generated two monoclonal antibodies that bind to the Sema- and VEGF-binding domains of NRP1, respectively. Both antibodies reduce angiogenesis and vascular remodeling, while having little effect on other VEGFR2-mediated events. Importantly, anti-NRP1 antibodies have an additive effect with anti-VEGF therapy in reducing tumor growth. Vessels from tumors treated with anti-VEGF show a close association with pericytes, while tumors treated with both anti-NRP1 and anti-VEGF lack this organization. We propose that blocking NRP1 function inhibits vascular remodeling, rendering vessels more susceptible to anti-VEGF therapy.

INTRODUCTION

Many proteins that were originally discovered to be required for axon guidance during neuronal development have been more recently shown to play critical roles in vascular development (Carmeliet and Tessier-Lavigne, 2005). One such family of axon guidance molecules is the semaphorin ligands and their receptors, the neuropilins (NRPs) and plexins. NRP1 was first characterized as a semaphorin receptor mediating axon growth cone collapse (He and Tessier-Lavigne, 1997; Kolodkin et al., 1997). It was subsequently shown that NRP1 is also an isoform-specific VEGF receptor expressed on tumor and endothelial cells (ECs; Soker et al., 1998), prompting considerable efforts to understand the role of NRPs in vascular and tumor biology (Klagsbrun et al., 2002; Bielenberg et al., 2006).

Genetic studies have provided strong evidence that *Nrp1* is required for vascular morphogenesis. Loss of *Nrp1* function results in vascular remodeling and branching defects (Kawasaki et al., 1999), a phenotype that can be further enhanced by the loss of *Nrp2* function (Takashima et al., 2002). These results suggest that early in development *Nrp1* and *Nrp2* may have overlapping functions; however, the expression of each *Nrp* is partitioned later in development, with *Nrp1* being expressed primarily in

SIGNIFICANCE

Bevacizumab is an approved antiangiogenic therapy that has shown promise for reducing tumor growth and extending survival of patients, particularly when used in combination with chemotherapy. However, some tumors are less responsive to VEGF blockage, promoting the search for additional therapies to augment the effects of bevacizumab. This report describes the generation of antibodies targeting NRP1, which was originally discovered as a receptor for the neuronal chemorepellent semaphorin 3A but was subsequently shown to also bind VEGF. Interestingly, blocking NRP1 function selectively disrupts remodeling of developing vasculature and combines with anti-VEGF therapy to further reduce tumor growth. Based on these results, it is proposed that NRP1 antibodies may render tumor vessels more responsive to anti-VEGF therapy.

arteries, and *Nrp2* in veins and lymphatic vessels (Herzog et al., 2001; Yuan et al., 2002). Notably, loss of *Nrp2* function alone specifically impairs lymphatic development.

As *Nrp1* is expressed in many other cell types during development, the role of vascular *Nrp1* was addressed through the generation of an EC-specific knockout (Gu et al., 2003), which resulted in vascular defects similar to those seen in the null allele. Interestingly, this study also showed that Sema3A binding to NRP1 is not required for vascular development. In another study, defects were observed in the guidance of endothelial tip cells in the developing hindbrain in *Nrp1* KO embryos (Gerhardt et al., 2004).

Two broad hypotheses exist for how NRP1 acts to regulate EC function. First, it has been proposed that NRP1 enhances VEGF binding to VEGFR2, thus enhancing VEGFR2 signaling. This idea is supported by experiments in which VEGF effects were examined on ECs overexpressing VEGFR2, in the presence or absence of NRP1 expression. These comparisons show enhanced migration, VEGFR2 activation, and VEGF binding to cells expressing both receptors (Soker et al., 2002). However, data have been published that support the alternative possibility that NRP1 may signal independently of VEGFR2 to regulate EC migration and/or adhesion (Wang et al., 2003; Murga et al., 2005).

To begin to distinguish these hypotheses, we generated two high-affinity monoclonal antibodies that bind different domains of NRP1 and compared them in neuronal and EC assays. Our results provide evidence that NRP1 plays a key role in modulating EC motility, and that its function extends beyond its previously assigned role as an enhancer of VEGFR2 signaling. In addition, we show that blocking NRP1 function can enhance the ability of anti-VEGF to block tumor growth, thus identifying NRP1 as a target for antitumor therapy in combination with anti-VEGF.

RESULTS

Generation of Phage-Derived Monoclonal Anti-NRP1 Antibodies

To distinguish between NRP1-mediated responses to semaphorin and VEGF on endothelial cells (ECs), we generated two high-affinity phage-derived monoclonal antibodies (mAbs) designed to block the function of each NRP1 ligand. One mAb was targeted to the primary region for Sema3A binding, the CUB (or a1–a2) domains, termed anti-NRP1^{A}; and another mAb was targeted to the primary region for VEGF binding, the coagulation V/VIII factor (or b1–b2) domains, termed anti-NRP1^{B} (Figure 1A). A detailed description of the generation and screening for anti-NRP1 mAbs will be discussed elsewhere (Liang et al., 2007). Both anti-NRP1 mAbs bind with similar affinities to human and murine NRP1 (Figure 1B; human NRP1 shown) but do not bind to NRP2 (data not shown). Anti-NRP1^{A} binds to murine and human NRP1 with a K_d of 7.8 nM and 0.9 nM, respectively, whereas anti-NRP1^{B} binds to murine and human NRP1 with a K_d of 1.3 nM and 0.4 nM, respectively.

Selective Actions of Anti-NRP1^{A} and Anti-NRP1^{B} on Sema3A Function and VEGF Binding

We tested the ability of each anti-NRP1 mAb to block binding of $VEGF_{165}$ to NRP1 in both an ELISA format and cell-based binding. Anti-NRP1^{B} strongly blocked VEGF binding to NRP1 and ECs, whereas anti-NRP1^{A} did not (Figures 1C and 1D). These results fit with the observation that the a1–a2 domains of NRP1 are not necessary for VEGF binding (Gu et al., 2002).

We next examined the effect of the antibodies on Sema3A function. It has been previously suggested that Sema3A and $VEGF_{165}$ may share overlapping binding domains in the N-terminal region of the b1 domain, and thus may compete for binding to NRP1 (Gu et al., 2002; Miao et al., 1999). Therefore, it seemed possible that a single anti-NRP1 mAb would block both Sema3A and VEGF binding. We tested the ability of our anti-NRP1 mAbs to block Sema3A-induced axon growth cone collapse. Dorsal root ganglia (DRG) were dissected from mouse E12.5 embryos and cultured to establish sensory neuron growth cones that were responsive to Sema3A/NRP1-dependent collapse (He and Tessier-Lavigne, 1997). Adding Sema3A to these cultures caused growth cones to retract their actin-rich structures (Figure S1A, arrowheads, in the Supplemental Data available with this article online). However, if anti-NRP1^{A} was added at the same time as Sema3A, collapse was completely blocked (Figure S1B). In contrast, anti-NRP1^{B} had no effect on Sema3A-induced collapse.

These two mAbs thus have functionally distinct actions: anti-NRP1^{A} blocks Sema3A function but does not interfere with VEGF binding to NRP1, whereas anti-NRP1^{B} blocks VEGF binding to NRP1 without effect on Sema3A function. Further studies showed that neither mAb blocks Sema3F/NRP2-dependent collapse of E17 hippocampal growth cones (Figure S1B), consistent with the observation that neither mAb binds NRP2. These mAbs thus provide selective tools to dissect the role of NRP1 in vascular biology.

Both Anti-NRP1^{A} and Anti-NRP1^{B} Reduce $VEGF_{165}$-Dependent Endothelial Cell Migration and Bead Outgrowth

We next investigated the role of NRP1 in VEGF-driven EC migration. Using a transwell system, human umbilical vein endothelial cells (HUVECs) were introduced into the top chamber, while VEGF was added to the bottom chamber to promote EC migration. ECs that had migrated to the bottom chamber were then quantified (Figure 2A). An anti-VEGF mAb was used as a positive control to block VEGF-driven EC migration (the cross-species reactive anti-VEGF mAb B20.4.1 was used in all experiments unless stated otherwise; Liang et al., 2006).

To determine whether NRP1 function is required for EC migration, anti-NRP1 mAbs were added to cells in the top chamber just prior to the addition of VEGF. Interestingly, both anti-NRP1^{A} and anti-NRP1^{B} significantly reduced EC migration, with anti-NRP1^{B} providing a stronger block of migration (Figure 2A). Similar results were obtained

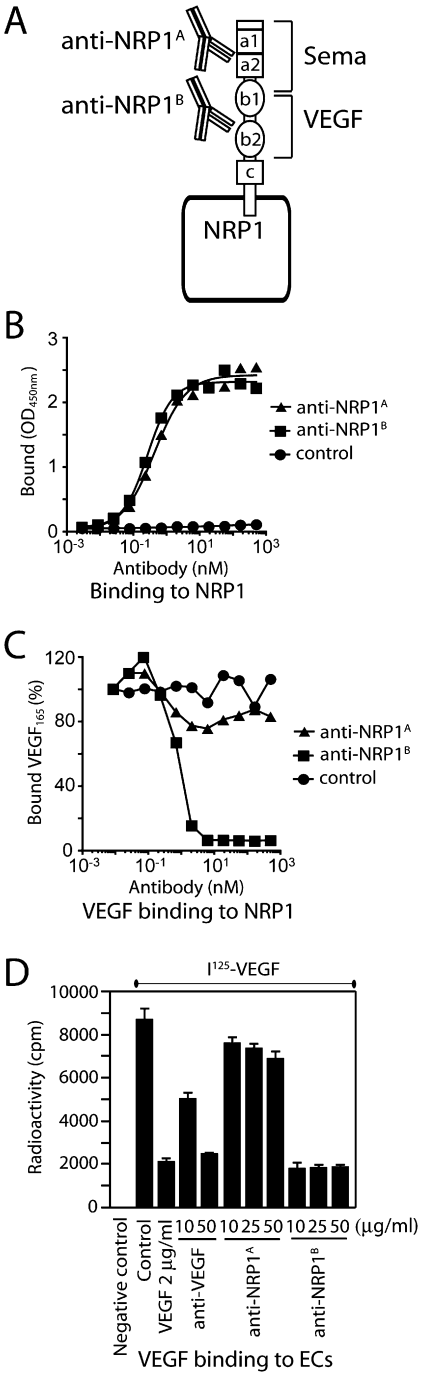

Figure 1. Characterization of Anti-NRP1^A and Anti-NRP1^B Antibodies

(A) Schematic representation of Sema- and VEGF-binding regions on NRP1 relative to anti-NRP1^A and anti-NRP1^B epitope regions.

(B) ELISA assay detecting binding of anti-NRP1^A and anti-NRP1^B to hNRP1.

(C) Blocking of VEGF binding to NRP1 by anti-NRP1 antibodies. Increasing amounts of anti-NRP1^A or anti-NRP1^B were preincubated with plates coated with human NRP1.Fc (5 μg/ml; NRP1 including a1,a1, b1,b2,c fused to human Fc) for 1–2 hr, followed by the addition of pretitrated biotinylated human VEGF$_{165}$ (1 nM) for 15 min. The percentage of bound VEGF$_{165}$ was detected by streptavidin-HRP conjugates.

(D) Blocking of I^{125}-VEGF$_{165}$ binding to HUVECs. Cells were incubated with control and anti-NRP1 antibodies at the indicated concentrations for 30 min followed by incubation with 0.1 nM I^{125}-VEGF$_{165}$ for 2 hr at 4°C. n = 3 for each condition.

using two other types of EC lines, HUAECs and HAECs (data not shown).

To further dissect the role of NRP1 in more complex EC functions, we employed an in vitro system of angiogenic sprouting (Nakatsu et al., 2003). ECs coated on beads sprout over a 7 day period, resulting in multiple well-defined vessel structures protruding from each bead (Figure 2B; control). Adding either anti-NRP1 mAbs to these cultures resulted in a reduction in vessel length, with anti-NRP1^B also showing a decrease in the number of sprouts (Figures 2B and 2C). Anti-VEGF was used as a positive control and completely blocked sprouting in this assay.

The finding that anti-NRP1^B interferes with VEGF actions was perhaps not surprising, since it blocks VEGF binding to NRP1, but the finding that anti-NRP1^A also affects VEGF function was unexpected, since it does not interfere with VEGF binding to NRP1. There are several possible explanations for why an antibody targeting the semaphorin-binding region of NRP1 would affect EC behavior. First, it seemed possible that anti-NRP1^A promotes NRP1 internalization. To address this possibility, we preincubated ECs with anti-NRP1^A at 37°C for either 5 min, 2 hr, or 20 hr, and then performed FACS analysis with anti-NRP1^B to determine the level of NRP1 on the cell surface (Figure S2A). No difference was observed between treatments, suggesting that anti-NRP1^A did not cause significant internalization of NRP1. Similar results were seen with anti-NRP1^B (Figure S2B).

A second possible explanation for why the anti-NRP1 mAbs reduce EC migration is that they might reduce EC adhesion to the extracellular matrix and/or reduce EC motility in general. It has been reported that NRP1 is required for cell attachment (Murga et al., 2005), and migration defects could be secondary to such an affect. Therefore, we examined the effects of the anti-NRP1 mAbs on EC adhesion to fibronectin, an extracellular matrix substrate; no defects were observed as compared to control mAbs (Figure S2C). To determine whether the anti-NRP1 mAbs disrupt EC motility generally, we examined whether they reduce migration of ECs in response to other growth factors but found that they did not block migration induced by either bFGF or HGF (Figure S2D; HGF data not shown).

Lastly, it has been reported that Sema3A regulates EC migration and adhesion (Miao et al., 1999), and that Sema3A may act in an autocrine manner to modulate EC adhesion through inhibiting integrin function (Serini et al., 2003). We tested this possibility by employing the same Sema3A used in the neuronal growth cone collapse assays shown in Figure S1, in EC assays. We observed no block of EC adhesion or migration in the presence of different concentrations of Sema3A (Figure S3) and therefore could not further examine the possibility that anti-NRP1^A acts by inhibiting Sema3A function on ECs.

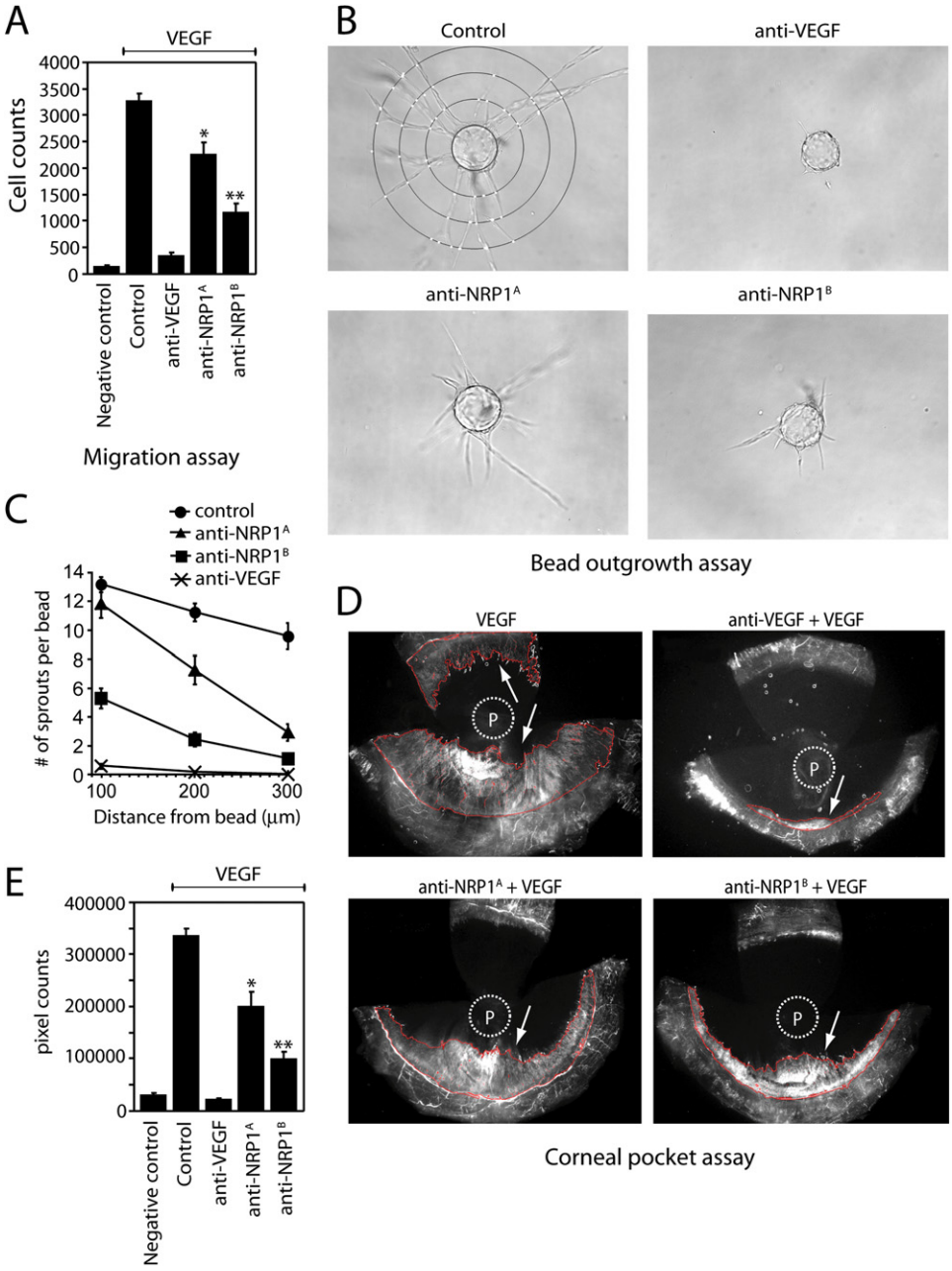

Figure 2. Anti-NRP1 mAbs Reduce VEGF-Induced Migration, In Vitro Sprouting, and In Vivo Neovascularization

(A) HUVECs with indicated mAbs (10 μg/ml) were allowed to migrate in the presence or absence of 10 ng/ml VEGF overnight. Quantification of migration assay (n = 6 for each condition). *p = 0.00003, **p = 0.1×10^{-10}.

(B) Endothelial bead sprouting assay with concentric rings drawn at 100, 200, and 300 μm from the center of the bead.

(C) Quantification of bead sprouting assay; n = 12–14 beads per condition. Sprouts were marked if they passed each respective line, giving an average number of sprouts at each given length.

(D) Representative corneal images illustrating the effects of intraconjunctival injection of indicated antibody (10 mg/kg) on VEGF-induced angiogenesis. VEGF (150 ng) and antibody are both added to the pellet (P). Arrows point to area of neovascularization outlined in red.

(E) Quantification of the pixel counts from the circled areas in (D). Averages of the results from each condition were shown (n = 5–7). *p = 0.000004, **p = 0.7×10^{-9}.

Both Anti-NRP1 Antibodies Reduce Neovascularization in the Rat Corneal Pocket Assay

Having observed a strong reduction in EC migration and vessel sprouting by blocking NRP1 in the in vitro assays, we next examined whether NRP1 is required for in vivo angiogenesis. This was accomplished using the rat corneal pocket assay, in which pellets containing VEGF were added to the avascular cornea to induce neovascularization.

Vessels invading the cornea were labeled with FITC-dextran and then imaged. Anti-VEGF resulted in a complete block of neovascularization, and both anti-NRP1^A and anti-NRP1^B significantly reduced vessel ingrowth (Figures 2D and 2E).

NRP1 Is Necessary for Vascular Remodeling in the Mouse Retina

Phenotypes observed in the *Nrp1* knockout mice are consistent with a defect in vascular remodeling (Gu et al., 2003; Kawasaki et al., 1999; Takashima et al., 2002). We next tested the requirement of NRP1 for vascular remodeling by analyzing the effects of systemic treatment with the anti-NRP1 mAbs on the developing mouse retina, which allowed us to investigate the stereotyped events of vascular sprouting, remodeling, and maturation (Dorrell and Friedlander, 2006). At birth, an astrocytic network is in place to guide ECs sprouting from central retinal artery located near the optic nerve head (ONH). After one day of postnatal life (P1) the retinal vasculature has developed a morphogenic furrow in the nerve fiber layer (NFL), lying superficial to the ganglion cell layer, that begins to extend toward the edge of the retina in a concentric pattern, reaching halfway by P5 (Figure 3A). Over the next 3 days, the furrow continues to extend to the edge of the retina, while the vascular plexus closest to the ONH undergoes stereotyped remodeling, consisting of thinning of the vascular plexus into a refined capillary network in the NFL (Figure 3B), and sprouting of vessels into deeper layers of the retina (Figure 3F).

Antibodies were injected into neonatal mice beginning at P1, followed by injections every other day until retinas were collected at P5 and P8. To visualize the vasculature, retinas were stained with isolectin B4 (green; Figure 3C). While the refined capillary network of the IgG control group is well established between P5 and P8, this vascular remodeling is inhibited by both anti-NRP1 mAbs. We quantified this difference by comparing the vascular density from representative images taken of the NFL vascular network in regions adjacent to the ONH (Figure 3D). Because treatment with either anti-NRP1 mAb results in a strong inhibition of vascular remodeling, vascular density is significantly higher in both anti-NRP1^A- and anti-NRP1^B-treated retinas as compared to controls. Interestingly, the developmental furrow continues to extend in both anti-NRP1 mAb-treated retinas, with only a slight inhibition of extension in the anti-NRP1^B-treated animals (Figure 3E). This suggests that development of the retina is not generally inhibited, but that there is a specific block in vascular remodeling when treating with either anti-NRP1 mAb.

In contrast to anti-NRP1 mAbs, anti-VEGF treatment resulted in a reduction of retinal vascular density (Figures 3C and 3D). At a qualitative level, vessels in anti-VEGF-treated retinas have a reduced complexity at P8, a trend that is present at P5. These data suggest that anti-VEGF treatment results in block of initial sprouting and/or vascular regression. Interestingly, systemic delivery of anti-VEGF does not significantly reduce the extension of the vascular furrow (Figure 3E). This may be a result of poor mAb diffusion to the extending tip cells (Gerhardt et al., 2003).

Evaluating P8 retinas also allowed us to further investigate the effects of mAb treatment on angiogenic sprouting. Between P5 and P8, vessels begin to sprout from the NFL vascular network into deeper vascular layers resulting in the formation of the outer plexiform layer (OPL) vascular network, which is superficial to the outer nuclear layer and is the deepest vascular bed in the retina (Figure 3F). Later in development, sprouting from collaterals that gave rise to the OPL results in an intermediate vascular bed, termed the inner plexiform layer (IPL). Images taken from the OPL at P8 show an inhibition of sprouting by both anti-NRP1 mAbs, and anti-VEGF (Figure 3G). In the case of the anti-NRP1 mAbs, it remains to be determined whether inhibition of OPL vascular sprouting is an indirect consequence of blocking vascular remodeling of the NFL vascular plexus.

The different phenotypes observed in retinas taken from animals systemically treated with either anti-NRP1^A or anti-NRP1^B, as compared to anti-VEGF, suggest that NRP1 may regulate EC function by mechanisms other than enhancing VEGFR2 signaling.

Blocking NRP1 Function Has Little Effect on VEGFR2 Signaling

We next investigated the requirement of NRP1 in EC proliferation and vascular permeability—two defining cellular activities induced by VEGF. Remarkably, treatment with either anti-NRP1 mAb had no effect on VEGF-induced permeability, whereas anti-VEGF provided a strong block (Figures 4A and 4B). A similar trend was observed when testing for VEGF-induced EC proliferation, with anti-NRP1^A showing no block of proliferation, and anti-NRP1^B only a slight dose-responsive reduction (Figure 4C). These results support published data showing that siRNA knockdown of NRP1 in ECs results in only a partial inhibition of VEGF-induced proliferation (Murga et al., 2005) and suggests that NRP1's primary role in VEGF-driven EC behaviors is to mediate cell migration. Notably, the same nonsaturating concentration range of VEGF (10–20 ng/ml; Figure S4) was used in all in vitro cellular and signaling experiments.

We next studied the effect of anti-NRP1 mAbs on VEGFR2 signaling. VEGF binds to the second and third extracellular IgG domains of VEGFR2 and activates the receptor by autophosphorylation (Dougher and Terman, 1999; Takahashi et al., 2001). In contrast to anti-VEGF, which completely blocked VEGFR2 phosphorylation induced by VEGF, anti-NRP1^A did not significantly change VEGFR2 phosphorylation levels, whereas anti-NRP1^B resulted in only a modest reduction (Figure 4D).

Rather than regulating VEGFR2 phosphorylation level directly, NRP1 may act to modulate specific VEGFR2 pathways. To address this possibility, we studied the effect of anti-NRP1 mAbs on downstream signaling events mediated by VEGFR2. VEGFR2 has been shown to induce EC proliferation through activation of the mitogen-activated

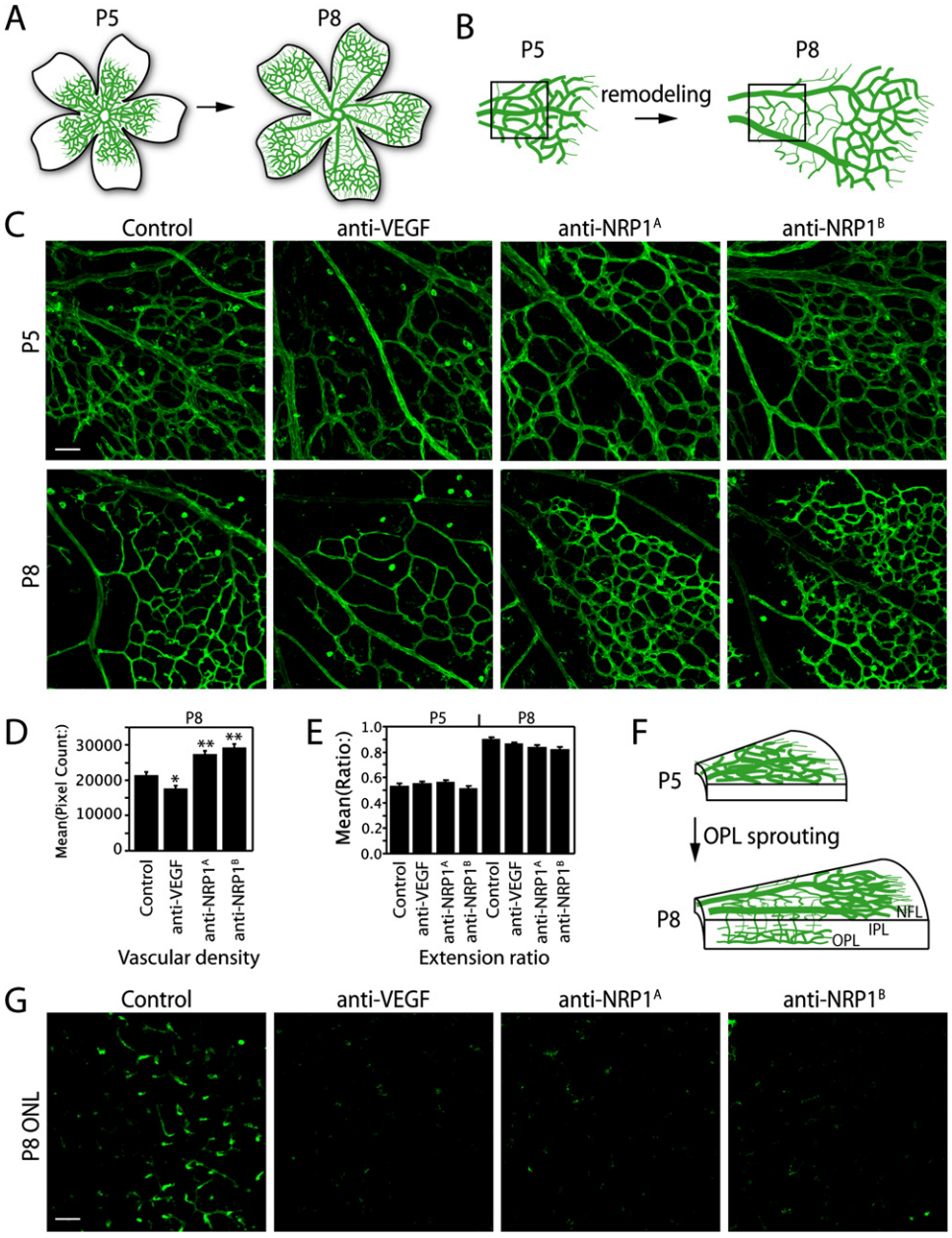

Figure 3. Anti-NRP1 mAbs Inhibit Vascular Remodeling in the Developing Retina

(A) Schematic of vascular development in the mouse retina from postnatal day 5 (P5) to P8. Vessels extend in a concentric patter to the retina edge. The optic nerve head (ONH) is located in the center of the retina.

(B) Vascular remodeling near the ONH takes place between P5 and P8. Images in (C) were acquired from areas boxed in schematic.

(C) Confocal images from the vascular RGC layer in control IgG-, anti-VEGF-, anti-NRP1^{A}-, and anti-NRP1^{B}-treated animals.

(D) Quantification of vascular density; total pixel count from 12 representative images from four treated retinas of each condition. *p = 0.006, **p < 0.0001.

(E) Quantification of vascular extension. Measured by the ratio of the distance from the ONH to the edge of the vasculature, over the distance from the ONH to the edge of retinal cup. Twelve representative measurements were taken from four treated retinas.

(F) Schematic of vascular sprouting into deeper layers of the retina. Vessels extend sprouts to the outer plexiform layer (OPL) and form a plexus. Later spouts arise between the NFL and OPL layers, eventually giving rise to the inner plexiform layer (IPL).

(G) Confocal images from the vascular OPL layer. Vasculature stained with isolectin B4. Scale bar, 50 μm (C and G).

protein kinases Erk1/2 (Rousseau et al., 1997; Takahashi et al., 1999), and to regulate EC survival and vascular permeability through the PI3-kinase/Akt pathway (Chen et al., 2005; Gerber et al., 1998; Six et al., 2002). Consistent with the observation that anti-NRP1 mAbs did not significantly change VEGF-induced EC proliferation or vascular

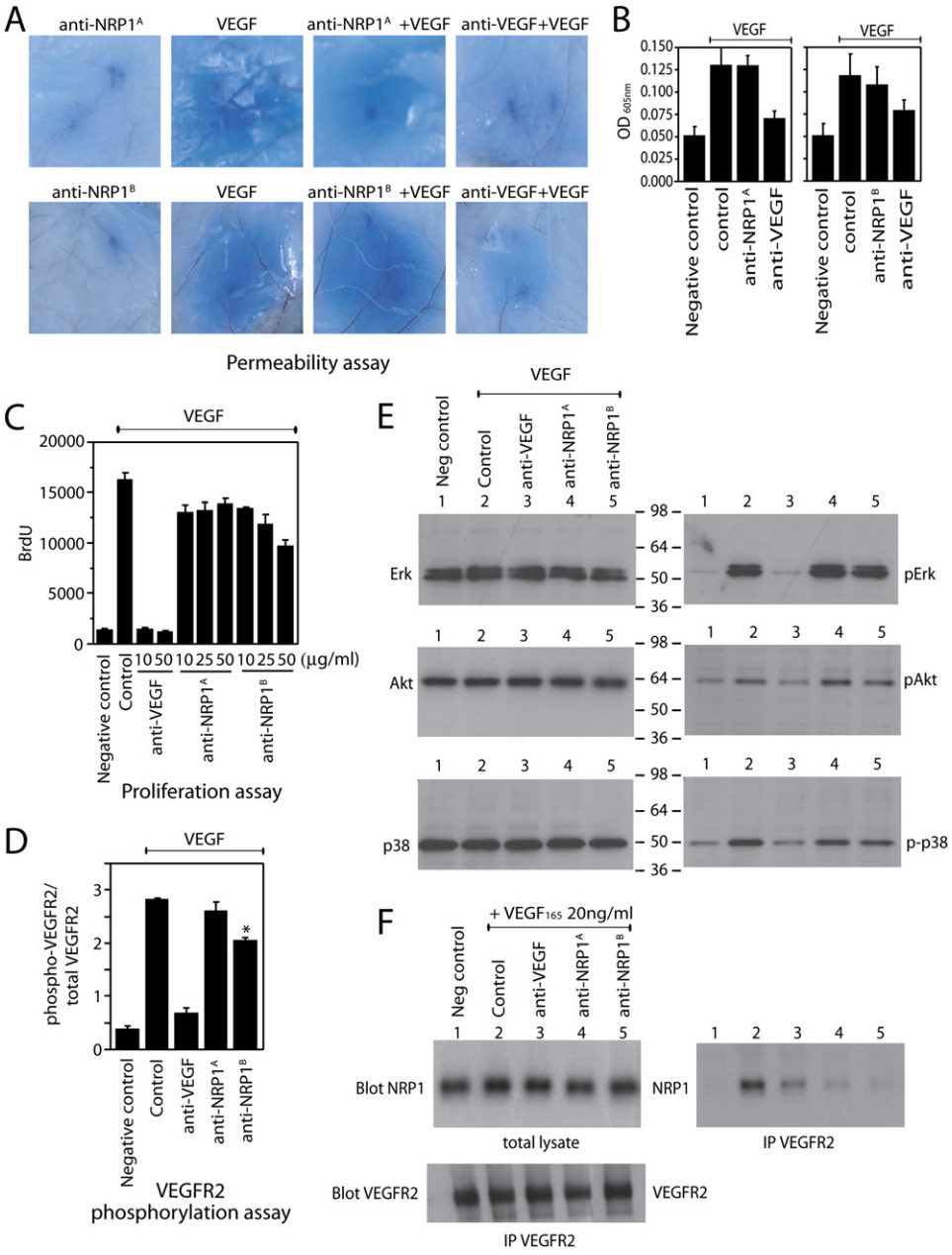

Figure 4. Effects of Anti-NRP1 mAbs on VEGF-Induced Vascular Permeability, HUVEC Proliferation, VEGFR2 Phosphorylation, and VEGFR2 Downstream Signaling

(A) Mouse skin vascular permeability assay. Images in the same row were taken from the skin of the same animal. Blue stain represents Evan's blue leakage from the vasculature.

(B) Quantification of the Evan's blue dye extracted from skin samples in the permeability assay. Values shown are the average of six independent experiments. Neither anti-NRP1^A- nor anti-NRP1^B-treated skin samples were significantly different from control ($p = 0.69$ for anti-NRP1^A, and $p = 0.989$ for anti-NRP1^B).

(C) Quantification of HUVEC proliferation in the presence or absence of 10 ng/ml VEGF as determined by BrdU incorporation ($n = 5$, each condition).

(D) VEGFR2 phosphorylation level in HUVECs detected by ELISA assay using antibodies that recognized total or tyrosine-phosphorylated VEGFR2. VEGF was added at 20 ng/ml for 10 min to induce the phosphorylation of VEGFR2; $n = 3$ for each condition. VEGFR2 phosphorylation level in anti-NRP1^A (10 μg/ml)-treated cells was not significantly different from that in the control group ($p = 0.1$). *$p = 0.0002$.

(E) Immunoblot analysis of HUVEC lysates. Cells were treated with the indicated antibodies at 50 μg/ml for 30 min, followed by a 10 min incubation with 20 ng/ml VEGF.

(F) Immunoprecipitation with anti-VEGFR2. Cells were treated with the indicated antibodies at 25 μg/ml for 30 min and then incubated with 20 ng/ml VEGF for 30 min on ice and then for 8 min at 37°C.

permeability, anti-NRP1^A and anti-NRP1^B incubation did not affect VEGF-induced phosphorylation of Erk1/2 or Akt. On the other hand, inhibiting NRP1 function with anti-NRP1 mAbs significantly reduced EC migration (Figure 2A). It is possible that NRP1 specifically regulates VEGFR2 pathways required for cell motility, such as the p38 MAP kinase pathway, which has been shown to be required for VEGF-driven actin reorganization and cell migration in ECs (Rousseau et al., 1997). Anti-NRP1^A and anti-NRP1^B treatments both resulted in a slight reduction in p38 phosphorylation level in HUVECs (Figure 4E). However, the mild decrease in p38 phosphorylation alone is unlikely to account for the strong reduction we observed in the migration and sprouting assays (Figure 2) or explain the qualitatively different phenotypes observed between the anti-NRP1 mAbs and anti-VEGF mAb treatments in the retinal vascular remodeling experiments (Figure 3).

Lastly, we tested the effect of anti-NRP1 mAbs on VEGF/NRP1/VEGFR2 complex formation. As reported previously (Soker et al., 2002), in the presence of VEGF, NRP1 can be coimmunoprecipitated from HUVEC lysate with anti-VEGFR2 antibodies (Figure 4F, lane 2). This interaction was reduced by anti-VEGF (Figure 4F, lane 3). Interestingly, both anti-NRP1^A and anti-NRP1^B strongly inhibit the formation of the NRP1/VEGFR2 complex (Figure 4F, lane 4 and 5). This observation is surprising, as anti-NRP1^A did not alter VEGF binding to NRP1 or ECs (Figures 1C and 1D), and had little effect on VEGFR2 activation or downstream signaling. These results suggest that anti-NRP1^A and anti-NRP1^B may be acting via the same mechanism to inhibit VEGF-driven motility events (i.e., by disrupting the NRP1/VEGFR2 complex).

Anti-NRP1 in Combination with Anti-VEGF Shows an Additive Effect in Reducing Tumor Growth

Blocking the VEGF pathway has been proven to reduce neovascularization in mouse tumor models and in human cancers (Ferrara and Kerbel, 2005). However, it is believed that some tumors are less dependent on VEGF for vessel formation or may become insensitive to anti-VEGF therapies (Jain et al., 2006; Kerbel et al., 2001). To determine if NRP1 blockade could enhance the tumor growth inhibition (TGI) provided by blocking VEGF, we selected several xenograft models known to exhibit varying sensitivity to anti-VEGF therapy. Since mouse stromal VEGF, in addition to tumor-derived VEGF, has been shown to impact tumor growth, we used anti-VEGF mAbs that recognize both murine and human VEGF (Liang et al., 2006).

These experiments were designed to test the effect of blocking NRP1 alone (anti-NRP1^A in red, anti-NRP1^B in green, Figure 5), and in combination with anti-VEGF (anti-NRP1^A combination in purple, anti-NRP1^B combination in light blue, Figure 5). Also included were single-agent anti-VEGF (blue, Figure 5) and isotype control mAbs (black, Figure 5). SK-MES-1 is a NSCLC xenograft model that expresses NRP1 primarily in vascular and stromal tissue, with an intermediate level of expression in tumor cells (Figure 5A and Figure S5A; IHC control shown in Figure S5B). In this model, anti-VEGF provided a 52% TGI, single-agent anti-NRP1^B caused a 37% TGI, and anti-NRP1^A had no significant effect on TGI (see Experimental Procedures for calculation; Figure 5B).

Most striking was the additive effect seen with either anti-NRP1 mAb in combination with anti-VEGF. In combination with anti-VEGF, anti-NRP1^A increased the TGI to 70%, and anti-NRP1^B increased the TGI to 77% (Figure 5B). Similar results were obtained in the H1299 NSCLC xenograft model, which also expresses NRP1 in vascular and stromal tissue at high levels, but in tumor cells to a lesser extent (Figure 5A and Figure S5A). Single-agent anti-NRP1^B showed 39% TGI, anti-VEGF showed 28% TGI, and both in combination showed 51% TGI (Figure 5C).

Animals in the SK-MES-1 model were dosed to day 35 and followed to day 60 to examine the delay in tumor growth (animals were removed from the study when tumor sizes exceeded 1500 mm^3; no animals were removed as a result of toxicity). The Kaplan-Meier plot shows a significant effect of both anti-NRP1 mAb combination arms in delaying tumor growth as compared to single-agent arms (Figure 5D). Measurements of tumor growth delay (TGD; see Experimental Procedures for calculations) show no single-agent delay for anti-NRP1^A, a 24% TGD for anti-NRP1^B, 60% for anti-VEGF, 93% for anti-NRP1^A combination arm, and 96% for anti-NRP1^B combination arm.

Blocking NRP1 Function Alters Tumor Vascular Morphology and Further Reduces Vascular Density in Combination with Anti-VEGF

To determine if blocking NRP1 may alter tumor cell function directly, we assayed the effects of anti-NRP1 mAbs on SK-MES-1 tumor cell proliferation and antibody-dependent cell-mediated cytotoxicity (ADCC; Figure S6). FACS analysis of the SK-MES-1 cell line confirms that NRP1 is the predominant VEGF receptor, and VEGFR3 is moderately expressed, while VEGFR1, VEGFR2, and NRP2 showed little expression (Figure S6A). VEGF had no effect on SK-MES-1 tumor cell proliferation. Likewise, anti-NRP1 mAb alone or in combination with anti-VEGF did not alter proliferation of SK-MES-1 tumor cells in vitro (Figure S6B). Next, we tested if anti-NRP1 mAbs may induce ADCC in an in vitro cellular model. Using anti-HER2 as a positive control in BT-474 tumor cells, we observed that anti-NRP1 mAbs did not induce cytotoxicity in either the BT-474 or SK-MES-1 cell lines (Figure S6C). These results suggest that anti-NRP1 mAbs inhibit SK-MES-1 tumor growth mainly by altering vessels.

To further evaluate the vascular changes in SK-MES-1 tumors, an additional study was performed, and tumors were harvested within the same time window for histological analysis (Figure 6A). Interestingly, both anti-NRP1^B and anti-VEGF significantly reduced vascular density, while combination treatment resulted in further reduction of vascular density (Figure 6B; vessels were analyzed from the peripheral ridge of viable tissue). Although we did not see an effect on SK-MES-1 tumor cell proliferation in vitro (Figure S6B), the further reduction of vascular density caused by the combination treatment resulted in a reduction of tumor cell proliferation in vivo (Figure S7).

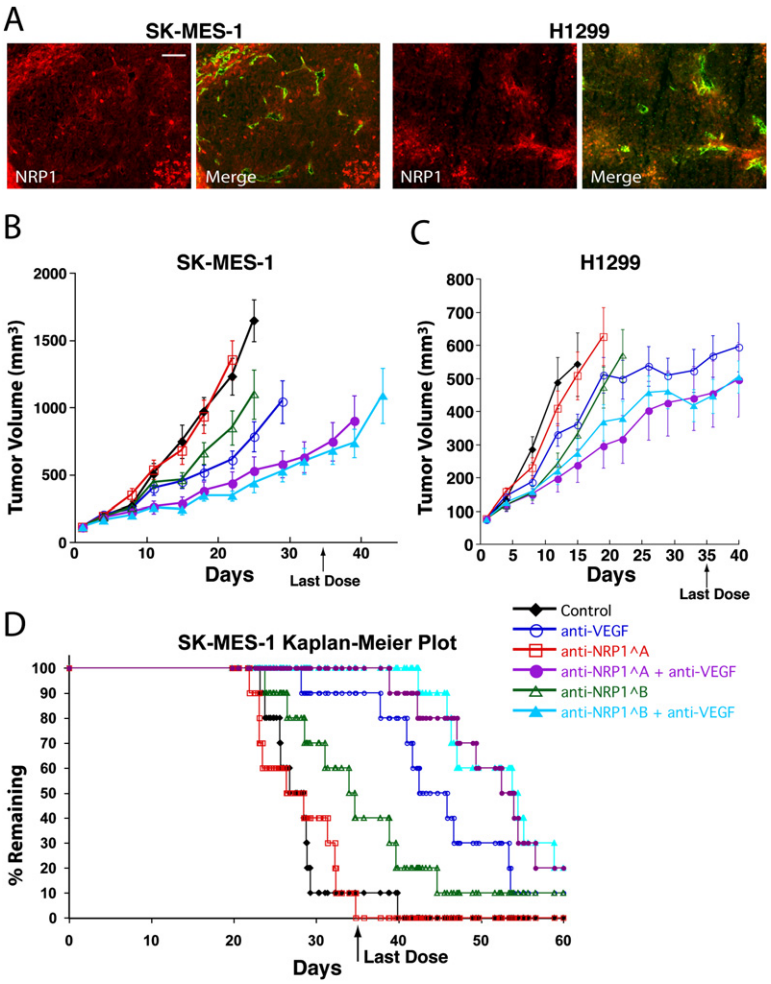

Figure 5. Human Xenograft Tumor Models Showing Single-Agent and Additive Effect of Anti-NRP1 mAbs in Combination with Anti-VEGF

(A) Immunohistochemistry of NRP1 (red) in SK-MES-1 and H1299 control tumor sections. PECAM is shown in green. Scale bar, 100 μm.

(B and C) Mean tumor volume graph of the SK-MES-1 (B) and H1299 (C) tumor models. Animals were dosed twice weekly i.p. with 10 mg/kg anti-NRP1 and/or 5 mg/kg of anti-VEGF or control antibody for 5 weeks.

(D) Kaplan-Meier plot for the SK-MES-1 tumor model.

We next investigated differences in vascular morphology among the various treatment groups (Figure 6C). Control IgG-treated tumors had large unorganized vessels, which were surrounded by pericytes, but lacked the wrapping morphology often seen when staining with anti-αSMA. Vessels in anti-VEGF-treated tumors showed not only a significant decrease in vascular density, but also a very close association with pericytes. Importantly, vessels in tumors treated with anti-NRP1^{B} and anti-VEGF in combination lacked close pericyte associations, while showing a stronger vascular density reduction than those tumors treated with anti-VEGF alone. These observations were confirmed by quantification of pericyte/vessel ratios (Figure 6D).

Although control and anti-VEGF tumors shared similar pericyte-to-vessel ratios in the SK-MES-1 model, anti-VEGF-treated tumor vessels were qualitatively different from the other treatment groups. The majority of vessels in the anti-VEGF-treated tumors showed a tight pericyte wrapping morphology (Figure 6E; arrows), a phenotype that was rarely observed in the other treatment groups. Similar results were also obtained in the Fo5, allograft murine breast tumor model (Figure S8). However in this model, tumors treated with control IgG (Figure S8C), as well as anti-NRP1 and combination treatments (Figures S8E and S8F), lacked pericyte coverage altogether, whereas anti-VEGF-treated tumors showed a massive increase in pericyte coverage (Figure S8D, quantified in Figure S8I). Additionally, Fo5 tumors analyzed by H&E staining appeared to show an increase in necrosis upon anti-NRP1 and anti-VEGF combination treatment (Figure S9).

Blocking NRP1 Function in Combination with Anti-VEGF in the Developing Retina Enhances Vascular Regression

Having observed that combining anti-NRP1 with anti-VEGF in tumors results in tumor vessels that lack features of maturation, including pericyte investment (Figure 6), and in light of results showing that NRP1 is required for vascular remodeling in the developing retina (Figure 3), we propose a model in which blocking NRP1 function in newly formed vessels inhibits vessels from undergoing remodeling and subsequent maturation, rendering vessels dependent on VEGF for survival (Figure 7A). A prediction of this model would be that combining anti-NRP1 with anti-VEGF in the developing retina would result in a stronger reduction in vascular density compared to

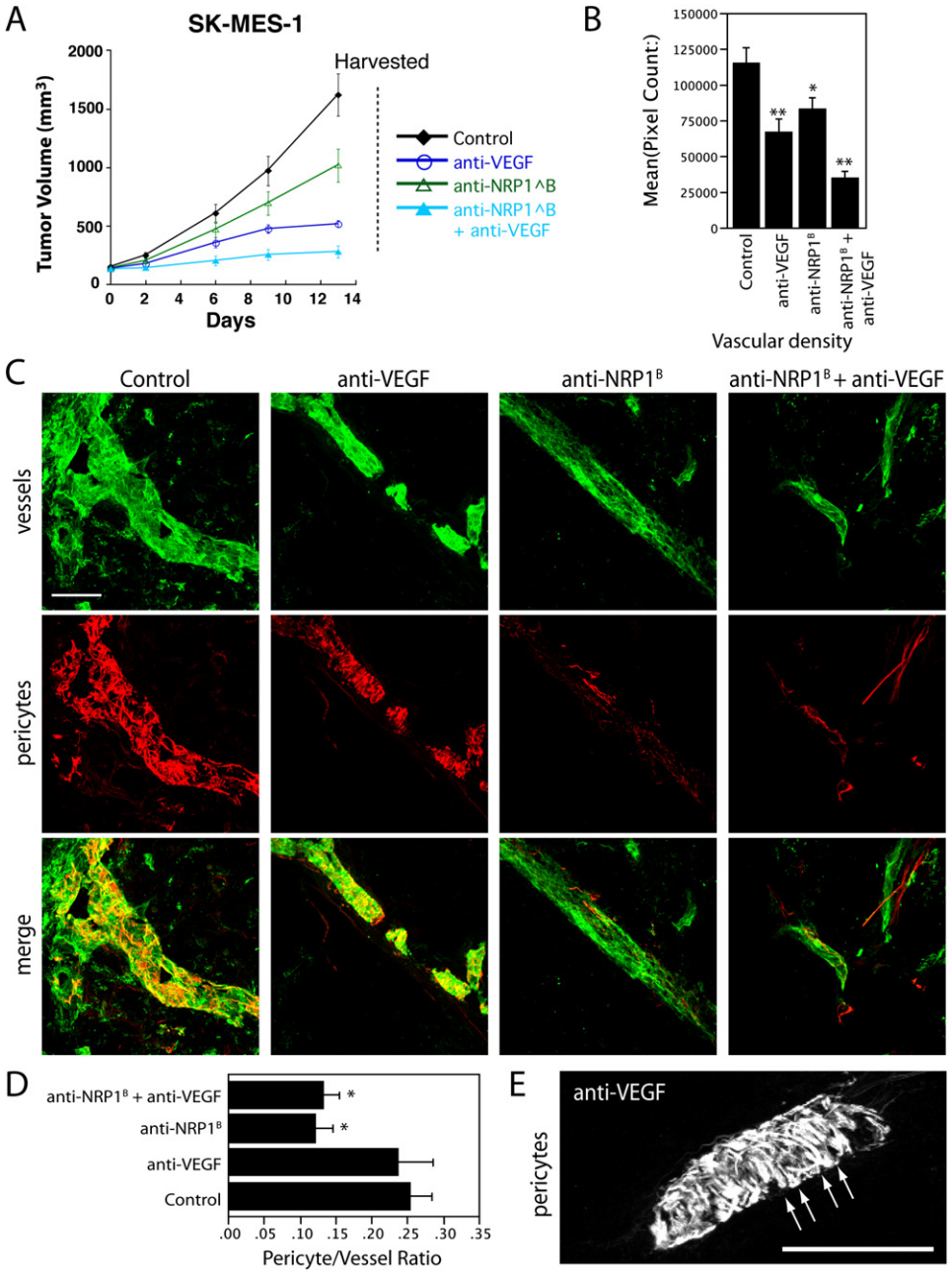

Figure 6. Anti-NRP1^B in Combination with Anti-VEGF Reduces Vascular Density and Pericyte Association with Vessels in Tumors

(A) Mean tumor volume graph of the SK-MES-1 tumor model. Model was repeated to harvest animals at the same time (dashed line, harvested after day 14) to compare vascular density and architecture. Animals were dosed as described in Figure 5.

(B) Quantification of vascular density. All three treatments reduce vascular density as compared to control: anti-VEGF, **p = 0.001; anti-NRP1^B, *p = 0.01; and combination of anti-NRP1^B + anti-VEGF, **p < 0.001. Difference between anti-VEGF and anti-NRP1^B + anti-VEGF is p = 0.03, whereas the anti-NRP1^B compared to anti-VEGF is not statistically significant (n = 6–10 images from 2–3 representative tumors; mean pixel number calculated using Image J).

(C) Confocal images of representative vessels (green; PECAM, ICAM, MECA32 combination stain) and pericyte (red; anti-αSMA) in treated tumors compared to control.

(D) Quantification of pericyte/vessel ratio. Anti-NRP1^B and anti-NRP1^B + anti-VEGF combination shows less pericyte coverage as compared to anti-VEGF treatment alone (*p = 0.02 and *p = 0.05, respectively).

(E) Confocal image of pericyte coverage in anti-VEGF-treated tumors. Arrows point to tight wrapping of pericytes in anti-VEGF-treated tumors. Scale bar, 50 μm (C and E).

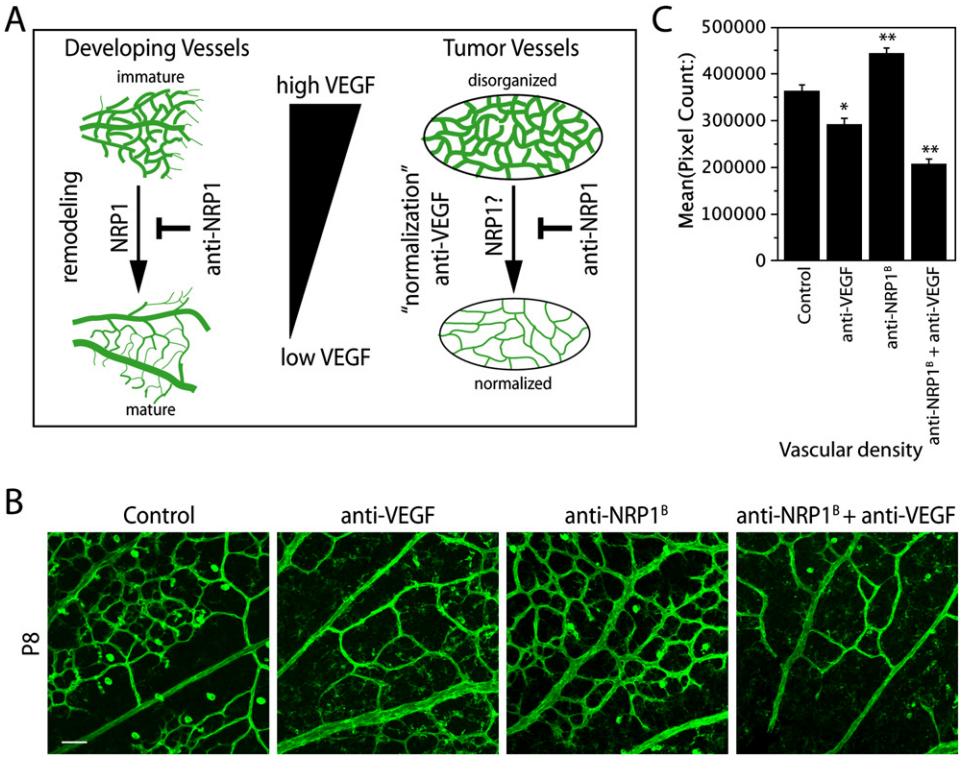

Figure 7. Potential Model for Additive Effects Seen with Anti-NRP1 and Anti-VEGF

(A) Using developing vessels as a model, we show that NRP1 is required for vascular remodeling. The transition from immature to mature vessels results in decreased VEGF dependency for vessel survival. In tumors, addition of anti-VEGF forces vessels into a VEGF-independent state, similar to what is seen naturally during vessel development. We hypothesize that blocking NRP1 in tumors will keep vessels from maturing, thus making tumor vessels more dependent on VEGF for survival. Therefore, combining anti-NRP1 with anti-VEGF results in further reduction in tumor vessels and subsequent inhibition of tumor growth.

(B) Confocal images showing combination treatment in neonate mice with anti-NRP1^B and anti-VEGF results in further vascular regression in the developing retina. Images are shown at P8; treatment is as described for Figure 3 (exception: anti-VEGF and anti-NRP1^B are dosed half of single agent alone [5 mg/kg versus 10 mg/kg single agent]). Scale bar, 50 μm.

(C) Quantification of vascular density. Compared to control, anti-VEGF reduces vascular density (*$p = 0.0004$), anti-NRP1^B increases vascular density (**$p < 0.0001$), and combination of anti-NRP1^B + anti-VEGF further decreases vascular density (**$p < 0.0001$). Difference between anti-VEGF and anti-NRP1^B + anti-VEGF combination is also highly significant (**$p < 0.0001$).

anti-VEGF treatment alone, as was shown in the SK-MES-1 tumor model (Figure 6B). To test this possibility, we treated neonate mice with both anti-NRP1^B and anti-VEGF in combination. Strikingly, the anti-NRP1^B + anti-VEGF combination treatment resulted in a massive decrease in vascular density (Figure 7B, quantified in Figure 7C; $p < 0.001$ when comparing anti-NRP1^B + anti-VEGF to anti-VEGF alone; 100,000–150,000 mean pixel density is contributed by major vessels that are not effected by treatment). These data combined with the additive effect seen in the tumor models suggest that anti-NRP1 mAb treatments augment anti-VEGF therapy by further regressing vessels.

DISCUSSION

NRP1 May Act Independently or in Parallel with VEGFR2 to Mediate EC Migration

We found scant evidence that either anti-NRP1 mAb affects VEGFR2 phosphorylation and downstream signaling. Using the same concentration of VEGF used in the migration and bead outgrowth assays, we observed only a mild reduction in EC proliferation, VEGFR2 phosphorylation, and p38-MAPK phosphorylation with anti-NRP1^B, and no reduction with anti-NRP1^A (Figure 4; see Figure S4 for VEGF dose response).

Results obtained using the anti-NRP1^B mAb, which blocks VEGF binding to NRP1, supports a mechanism where one of NRP1's roles is to enhance VEGFR2 signaling, but only to a modest extent, a conclusion supported by a recent report showing that a peptide designed to block $VEGFA_{165}$ binding to NRP1 reduces VEGF cross-linking to VEGFR2 and decreases VEGFR2 activation (Jia et al., 2006). One explanation for the modest effects of anti-NRP1^B on EC proliferation and vascular permeability is that different VEGF-induced physiological events might require differential levels of VEGFR2 activation. Thus, the slight decrease in VEGFR2 phosphorylation may be sufficient to inhibit EC migration, while having little effect on permeability and proliferation.

Having observed that blocking NRP1 function with our anti-NRP1 mAbs only has a slight effect on canonical VEGFR2 signaling (Cross et al., 2003), we investigated other mechanisms by which blocking NRP1 function may effect VEGF-driven motility. In particular, we were surprised by the result that an antibody targeting the Sema-binding region of NRP1, which does not affect VEGF binding to NRP1, could reduce VEGF-driven motility events (Figure 2). This did not appear to result from internalization of NRP1, from a decrease in adhesion, or from a general decrease in motility of ECs (Figure S2). Likewise, we were unable to observe any effects of Sema3A on EC migration or adhesion, contrary to previous reports (Figure S3; Miao et al., 1999; Serini et al., 2003). Therefore, it is unlikely that the reduction in VEGF-induced motility using anti-NRP1^{A} can be explained by disrupting the proposed Sema3A autocrine loop, in which EC-expressed Sema3A regulates adhesion by modulating integrin function (Serini et al., 2003).

Lastly, we asked if blocking NRP1 function disrupts the VEGF/NRP1/VEGFR2 complex. As expected, blocking VEGF binding to NRP1 using anti-NRP1^{B} completely blocks the formation of this complex (Figure 4). Surprisingly, anti-NRP1^{A} also strongly inhibits the formation of this complex. In light of the fact that anti-NRP1^{A} does not effect VEGF binding to NRP1 or VEGFR2 signaling, these data suggest that disrupting NRP1 association with activated VEGFR2 selectively disrupts EC migration, further supporting a model in which NRP1 brings unique machinery to the VEGFR2 complex, acting in parallel with or independently of VEGFR2 to regulate EC motility. One molecular candidate regulating this process is NIP (GIPC), a PDZ domain-containing protein that interacts directly with NRP1 and potentially plays a role in vesicular trafficking (Cai and Reed, 1999; De Vries et al., 1998). Recent findings show that knocking down GIPC results in similar vascular defects as NRP1 knockdown in zebrafish (Wang et al., 2006).

Blocking NRP1 in Tumors Can Augment Anti-VEGF Effects

Our findings that anti-NRP1 mAbs and anti-VEGF may be acting by blocking different EC functions and/or signaling pathways raised the possibility that combining these antibodies in tumor models could have an additive effect in reducing tumor growth. Indeed, we observed a profound additive effect when combining anti-NRP1 with anti-VEGF (Figures 5 and 6). In the case of anti-NRP1^{A}, the results suggest a synergistic rather than additive effect, since in multiple tumor models the mean tumor volume following single-agent anti-NRP1^{A} treatment was not different from control; however, anti-NRP1^{A} in combination with anti-VEGF significantly enhanced tumor growth inhibition when compared with anti-VEGF alone.

In the case of anti-NRP1^{B}, single-agent treatment resulted in a significant reduction in tumor growth (Figures 5 and 6). Interestingly, these effects are only slightly less potent than anti-VEGF alone. However, the reduction in tumor growth from the combination arms for anti-NRP1^{B} were profound. We speculate that the single-agent effect of anti-NRP1^{B} is due to its relatively stronger inhibitory activity in reducing sprouting and in vivo angiogenesis, compared to anti-NRP1^{A}. On the other hand, we observed that both mAbs were equally potent in blocking vascular remodeling in the mouse retinal development assay (Figure 3) and inhibiting pericyte association with vessels in the Fo5 tumor model (Figure S8). We discuss these results in greater detail below.

NRP1 Is Required for Vascular Remodeling: A Potential Mechanism for Anti-NRP1 and Anti-VEGF Additive Effects

By systemic delivery of mAbs in neonatal mice, and analysis of retinal vascular development, we were able to investigate the role of NRP1 in vascular remodeling. Based on the *Nrp1* knockout phenotypes (Gu et al., 2003; Kawasaki et al., 1999; Takashima et al., 2002), we speculated that acute block of NRP1 function would result in the inhibition of vascular plexus remodeling. Although the extension of the developing vascular furrow was only slightly inhibited by treatment with either anti-NRP1 mAb, we observed a striking inhibition of vascular remodeling. These results are in contrast to the vessel architecture observed for anti-VEGF-treated animals, which resulted in a decrease in vascular complexity and density (Figure 3).

It has been proposed that vascular remodeling in the retina takes place in the absence of close pericyte associations, suggesting that pericytes serve to stabilize immature blood vessels ending the plasticity period of vessel remodeling (Benjamin et al., 1998). Our data suggest that NRP1 is required for this intricate process of vessel remodeling, consisting of the morphogenesis of the vascular plexus into fine capillaries, followed by further maturation. Unfortunately, we were unable to evaluate close pericyte associations in the capillary plexus region in these young animals, as pericytes are present but not uniformly organized into capillary beds until later time points in development. However, further analysis of retinas treated with either anti-NRP1 mAb or anti-VEGF showed that arterial and venous differentiation was not significantly altered (data not shown). Specifically, mAb treatment did not alter α-smooth muscle actin distribution on larger vessels at P5 or P8, suggesting that well-established vessels are not altered by anti-NRP1 or anti-VEGF treatment.

The idea of pericytes stabilizing tumor vessels, thus giving rise to anti-VEGF therapy resistance as a consequence of vessels losing their VEGF dependence, has been proposed and tested experimentally (Bergers et al., 2003; Erber et al., 2004). In these studies, it was observed that blocking both the function of VEGF (EC ligand) and PDGF (pericyte ligand) results in further disruption of tumor vasculature. Subsequently, it has been shown in elegant imaging studies that blocking VEGF function alone in tumors results in a significant amount of vascular regression; however, remaining vessels become "normalized" with close pericyte associations, possibly a consequence of immature vessels undergoing vascular remodeling and maturation (Inai et al., 2004).

Based on our observations in the developing retina, we hypothesized that blocking NRP1 function in tumors would also reduce vascular remodeling of tumor vessels in the presence of anti-VEGF, subsequently inhibiting vessel maturation, therefore keeping vessels in a state of VEGF dependence (model shown in Figure 7A). Inhibiting vessel remodeling alone may not have a significant effect on reducing tumor growth, as most tumor vessels are already inherently disorganized (Baluk et al., 2005). This prediction is consistent with the observation that, although anti-NRP1^{A} strongly inhibits vascular remodeling, we do not see a single-agent effect with this antibody in reducing tumor growth. However, we speculated that blocking vascular remodeling, and the subsequent maturation, in combination with anti-VEGF therapy may render the remaining tumor vessels more susceptible to regression. Our experiments showed that vessels remaining in tumors treated with anti-NRP1 mAbs in combination with anti-VEGF indeed lack pericyte association (Figure 6 and Figure S8). These results suggest that the additive effect we observe in blocking both NRP1 and VEGF function may arise as a consequence of rendering remaining vessels more vulnerable to regression induced by anti-VEGF therapy.

Finally, it is possible that NRP1 may also be required for pericyte function. It has recently been reported that bFGF induces upregulation of NRP1 on smooth muscle cells, resulting in the ability of VEGF to induce smooth muscle cell migration (Liu et al., 2005). In our own studies, we observed expression of NRP1 on human smooth muscle cells, as well as on pericytes in various murine and human tumors (for example, NRP1 expression extends to areas adjacent to vessels; Figure 5 and Figure S8). Possible roles for NRP1 in pericyte function remain to be explored.

NRP1 Expression on Tumor Cells

In addition to the vascular function of NRP1, which is the focus of this manuscript, others have reported a potential role for NRP1 expressed on tumor cells (Bielenberg et al., 2006). In fact, Klagsbrun and colleagues initially cloned NRP1 as a tumor cell-specific receptor for VEGF (Soker et al., 1998) and later proposed a model in which NRP1 receptors expressed on tumor cells act in *trans* to enhance tumor vascularization (Miao et al., 2000). Consistent with the positive role of NRP1 in tumorigenesis, some reports documented that the expression of NRP1 in various tumor types correlates with poor prognosis, advanced disease state, and invasiveness (Kawakami et al., 2002; Latil et al., 2000; Vanveldhuizen et al., 2003; Hansel et al., 2004), and in cell culture, increased expression of NRP1 on tumor cells was found to correlate with survival and chemoresistance (Bachelder et al., 2001; Wey et al., 2005). Other reports have, however, suggested that NRP1 is a negative regulator of tumorigenesis in some cases. In one study, expression of NRP1 in tumor cell lines that normally do not express NRP1 inhibits the tumorigenic phenotype of these cells (Gray et al., 2005). It also has been recently reported that maintained expression of NRP1 in colon cancer correlates with a better prognosis (Kamiya et al., 2006). These studies illustrate the complex function of NRP1 on tumors.

The tumor models we selected for this study show moderate to low expression of NRP1 on tumor cells (Figure 5; Figures S5 and S8). Likewise, we were unable to observe any effect on SK-MES-1 tumor cell proliferation or induction of ADCC with our anti-NRP1 mAbs. Nonetheless, we cannot dismiss the possibility that the additive effect we observe in reducing tumor growth is in part a consequence of affecting tumor cell function.

Conclusion

We show that blocking both NRP1 and VEGF function in tumor models results in an additive effect in reducing tumor growth. We also present evidence that NRP1 may also be acting through mechanisms other than VEGFR2 signaling. These data are both unexpected and intriguing and suggest that blocking NRP1 function may be a useful approach for enhancing antiangiogenic therapy.

EXPERIMENTAL PROCEDURES

Bead Outgrowth Assay

Dextran-coated Cytodex 3 microcarrier beads (Amersham) were incubated with HUVECs (400 cells per bead) in EGM-2, which contains 2 ng/ml VEGF, overnight at 37°C. To induce clotting, 0.5 ml cell-coated beads in PBS with 2.5 μg/ml fibrinogen (200 beads/ml) was added into one well of a 24-well tissue culture plate containing 0.625 units thrombin and incubated for 5 min at room temperature and then for 20 min at 37°C. The clot was equilibrated in EMG-2 for 30 min at 37°C. The medium was then replaced with EGM-2 containing skin fibroblast cells (Detroit 551, ~20,000 cells/ml). Antibodies were added to each well, and the assay was monitored for 8 days with change in medium every 2–3 days. Images of the beads were captured by an inverted microscope, and concentric circles spaced at 100, 200, and 300 μm were drawn around the bead in each image. The number of vessels crossing each line was counted.

Animal Studies

All studies were conducted in accordance with the Guide for the Care and Use of Laboratory Animals, published by the NIH (NIH Publication 85-23, revised 1985). An Institutional Animal Care and Use Committee (IACUC) approved all animal protocols.

Mouse Neonatal Retinal Vascular Assay

Neonatal CD1 mice were injected i.p. with mAbs at 10 mg/kg (5 mg/kg for combination study). The injections were performed on postnatal days 1 and 3 for P5 studies, and on days 1, 3, and 5 for P8 studies. Eyes were collected and fixed with 4% PFA. The dissected retinas were blocked with 10% mouse serum in PBSt (PBS, 1% Triton X-100) for 3 hr and then incubated overnight at 4°C with 25 μg/ml biotinylated isolectin B4 (Sigma) in PBLEC (1% Triton X-100, 0.1 mM $CaCl_2$, 0.1 mM $MgCl_2$, 0.1 mM $MnCl_2$, in PBS [pH 6.8]). Retinas were then washed and stained with Alexa 488 streptavidin (Molecular Probes). Images of flat-mounted retinas were captured by confocal fluorescence microscopy.

Tumor Models

For SK-MES-1, each HRLN female nude mouse received a 1 mm^3 tumor fragment s.c. implant in the flank. For H1299, 1×10^7 tumor cells were injected s.c. into the flank of HRLN female nude mice. Tumor growth was monitored twice weekly by caliper measurements. When tumors reached an average size of 80–120 mm^3, mice were sorted to give nearly identical group mean tumor sizes, and treatment was started. This was considered day 1 of each study. All treatments

were bodyweight-adjusted at 0.2 ml/20 g. For details on measurement of %TGI and %TGD, see statistical analysis in the Supplemental Data.

For details on other Experimental Procedures, see the Supplemental Data.

Supplemental Data

The Supplemental Data include Supplemental Experimental Procedures and nine supplemental figures and can be found with this article online at http://www.cancercell.org/cgi/content/full/11/1/53/DC1/.

ACKNOWLEDGMENTS

We thank K. Reif and T. Huang for generation of reagents. We thank Y. Lu, G. Meng, and H. Xiang for assay development and initial PK studies. We thank W. Ye, M. Yan, C. Wiesmann, E. Filvaroff, N. Ferrara, X. Wu, W. Mallet, R. Carano, J. Dela Cruz, K. Totpal, and A. Yaron for discussions and collaborative studies. All authors are full-time employees of Genentech, Inc.

Received: May 4, 2006
Revised: August 7, 2006
Accepted: October 31, 2006
Published: January 15, 2007

REFERENCES

Bachelder, R.E., Crago, A., Chung, J., Wendt, M.A., Shaw, L.M., Robinson, G., and Mercurio, A.M. (2001). Vascular endothelial growth factor is an autocrine survival factor for neuropilin-expressing breast carcinoma cells. Cancer Res. *61*, 5736–5740.

Baluk, P., Hashizume, H., and McDonald, D.M. (2005). Cellular abnormalities of blood vessels as targets in cancer. Curr. Opin. Genet. Dev. *15*, 102–111.

Benjamin, L.E., Hemo, I., and Keshet, E. (1998). A plasticity window for blood vessel remodelling is defined by pericyte coverage of the preformed endothelial network and is regulated by PDGF-B and VEGF. Development *125*, 1591–1598.

Bergers, G., Song, S., Meyer-Morse, N., Bergsland, E., and Hanahan, D. (2003). Benefits of targeting both pericytes and endothelial cells in the tumor vasculature with kinase inhibitors. J. Clin. Invest. *111*, 1287–1295.

Bielenberg, D.R., Pettaway, C.A., Takashima, S., and Klagsbrun, M. (2006). Neuropilins in neoplasms: Expression, regulation, and function. Exp. Cell Res. *312*, 584–593.

Cai, H., and Reed, R.R. (1999). Cloning and characterization of neuropilin-1-interacting protein: A PSD-95/Dlg/ZO-1 domain-containing protein that interacts with the cytoplasmic domain of neuropilin-1. J. Neurosci. *19*, 6519–6527.

Carmeliet, P., and Tessier-Lavigne, M. (2005). Common mechanisms of nerve and blood vessel wiring. Nature *436*, 193–200.

Chen, J., Somanath, P.R., Razorenova, O., Chen, W.S., Hay, N., Bornstein, P., and Byzova, T.V. (2005). Akt1 regulates pathological angiogenesis, vascular maturation and permeability in vivo. Nat. Med. *11*, 1188–1196.

Cross, M.J., Dixelius, J., Matsumoto, T., and Claesson-Welsh, L. (2003). VEGF-receptor signal transduction. Trends Biochem. Sci. *28*, 488–494.

De Vries, L., Lou, X., Zhao, G., Zheng, B., and Farquhar, M.G. (1998). GIPC, a PDZ domain containing protein, interacts specifically with the C terminus of RGS-GAIP. Proc. Natl. Acad. Sci. USA *95*, 12340–12345.

Dorrell, M.I., and Friedlander, M. (2006). Mechanisms of endothelial cell guidance and vascular patterning in the developing mouse retina. Prog. Retin. Eye Res. *25*, 277–295.

Dougher, M., and Terman, B.I. (1999). Autophosphorylation of KDR in the kinase domain is required for maximal VEGF-stimulated kinase activity and receptor internalization. Oncogene *18*, 1619–1627.

Erber, R., Thurnher, A., Katsen, A.D., Groth, G., Kerger, H., Hammes, H.P., Menger, M.D., Ullrich, A., and Vajkoczy, P. (2004). Combined inhibition of VEGF and PDGF signaling enforces tumor vessel regression by interfering with pericyte-mediated endothelial cell survival mechanisms. FASEB J. *18*, 338–340.

Ferrara, N., and Kerbel, R.S. (2005). Angiogenesis as a therapeutic target. Nature *438*, 967–974.

Gerber, H.P., Dixit, V., and Ferrara, N. (1998). Vascular endothelial growth factor induces expression of the antiapoptotic proteins Bcl-2 and A1 in vascular endothelial cells. J. Biol. Chem. *273*, 13313–13316.

Gerhardt, H., Golding, M., Fruttiger, M., Ruhrberg, C., Lundkvist, A., Abramsson, A., Jeltsch, M., Mitchell, C., Alitalo, K., Shima, D., and Betsholtz, C. (2003). VEGF guides angiogenic sprouting utilizing endothelial tip cell filopodia. J. Cell Biol. *161*, 1163–1177.

Gerhardt, H., Ruhrberg, C., Abramsson, A., Fujisawa, H., Shima, D., and Betsholtz, C. (2004). Neuropilin-1 is required for endothelial tip cell guidance in the developing central nervous system. Dev. Dyn. *231*, 503–509.

Gray, M.J., Wey, J.S., Belcheva, A., McCarty, M.F., Trevino, J.G., Evans, D.B., Ellis, L.M., and Gallick, G.E. (2005). Neuropilin-1 suppresses tumorigenic properties in a human pancreatic adenocarcinoma cell line lacking neuropilin-1 coreceptors. Cancer Res. *65*, 3664–3670.

Gu, C., Limberg, B.J., Whitaker, G.B., Perman, B., Leahy, D.J., Rosenbaum, J.S., Ginty, D.D., and Kolodkin, A.L. (2002). Characterization of neuropilin-1 structural features that confer binding to semaphorin 3A and vascular endothelial growth factor 165. J. Biol. Chem. *277*, 18069–18076.

Gu, C., Rodriguez, E.R., Reimert, D.V., Shu, T., Fritzsch, B., Richards, L.J., Kolodkin, A.L., and Ginty, D.D. (2003). Neuropilin-1 conveys semaphorin and VEGF signaling during neural and cardiovascular development. Dev. Cell *5*, 45–57.

Hansel, D.E., Wilentz, R.E., Yeo, C.J., Schulick, R.D., Montgomery, E., and Maitra, A. (2004). Expression of neuropilin-1 in high-grade dysplasia, invasive cancer, and metastases of the human gastrointestinal tract. Am. J. Surg. Pathol. *28*, 347–356.

He, Z., and Tessier-Lavigne, M. (1997). Neuropilin is a receptor for the axonal chemorepellent Semaphorin III. Cell *90*, 739–751.

Herzog, Y., Kalcheim, C., Kahane, N., Reshef, R., and Neufeld, G. (2001). Differential expression of neuropilin-1 and neuropilin-2 in arteries and veins. Mech. Dev. *109*, 115–119.

Inai, T., Mancuso, M., Hashizume, H., Baffert, F., Haskell, A., Baluk, P., Hu-Lowe, D.D., Shalinsky, D.R., Thurston, G., Yancopoulos, G.D., and McDonald, D.M. (2004). Inhibition of vascular endothelial growth factor (VEGF) signaling in cancer causes loss of endothelial fenestrations, regression of tumor vessels, and appearance of basement membrane ghosts. Am. J. Pathol. *165*, 35–52.

Jain, R.K., Duda, D.G., Clark, J.W., and Loeffler, J.S. (2006). Lessons from phase III clinical trials on anti-VEGF therapy for cancer. Nat. Clin. Pract. Oncol. *3*, 24–40.

Jia, H., Bagherzadeh, A., Hartzoulakis, B., Jarvis, A., Lohr, M., Shaikh, S., Aqil, R., Cheng, L., Tickner, M., Esposito, D., et al. (2006). Characterisation of a bicyclic peptide neuropilin-1 (NP-1) antagonist (EG3287) reveals importance of vascular endothelial growth factor exon 8 for NP-1 binding and role of NP-1 in KDR signalling. J Biol Chem. *281*, 13493–13502.

Kamiya, T., Kawakami, T., Abe, Y., Nishi, M., Onoda, N., Miyazaki, N., Oida, Y., Yamazaki, H., Ueyama, Y., and Nakamura, M. (2006). The preserved expression of neuropilin (NRP) 1 contributes to a better prognosis in colon cancer. Oncol. Rep. *15*, 369–373.

Kawakami, T., Tokunaga, T., Hatanaka, H., Kijima, H., Yamazaki, H., Abe, Y., Osamura, Y., Inoue, H., Ueyama, Y., and Nakamura, M. (2002). Neuropilin 1 and neuropilin 2 co-expression is significantly correlated with increased vascularity and poor prognosis in nonsmall cell lung carcinoma. Cancer *95*, 2196–2201.

Kawasaki, T., Kitsukawa, T., Bekku, Y., Matsuda, Y., Sanbo, M., Yagi, T., and Fujisawa, H. (1999). A requirement for neuropilin-1 in embryonic vessel formation. Development *126*, 4895–4902.

Kerbel, R.S., Yu, J., Tran, J., Man, S., Viloria-Petit, A., Klement, G., Coomber, B.L., and Rak, J. (2001). Possible mechanisms of acquired resistance to anti-angiogenic drugs: Implications for the use of combination therapy approaches. Cancer Metastasis Rev. *20*, 79–86.

Klagsbrun, M., Takashima, S., and Mamluk, R. (2002). The role of neuropilin in vascular and tumor biology. Adv. Exp. Med. Biol. *515*, 33–48.

Kolodkin, A.L., Levengood, D.V., Rowe, E.G., Tai, Y.T., Giger, R.J., and Ginty, D.D. (1997). Neuropilin is a semaphorin III receptor. Cell *90*, 753–762.

Latil, A., Bieche, I., Pesche, S., Valeri, A., Fournier, G., Cussenot, O., and Lidereau, R. (2000). VEGF overexpression in clinically localized prostate tumors and neuropilin-1 overexpression in metastatic forms. Int. J. Cancer *89*, 167–171.

Liang, W.C., Wu, X., Peale, F.V., Lee, C.V., Meng, Y.G., Gutierrez, J., Fu, L., Malik, A.K., Gerber, H.P., Ferrara, N., and Fuh, G. (2006). Cross-species vascular endothelial growth factor (VEGF)-blocking antibodies completely inhibit the growth of human tumor xenografts and measure the contribution of stromal VEGF. J. Biol. Chem. *281*, 951–961.

Liang, W.-C., Dennis, M.S., Stawicki, S., Chanthery, Y., Pan, Q., Chen, Y., Eigenbrot, C., Yin, J., Koch, A.W., Wu, X., et al. (2007). Function blocking antibodies to Neuropilin-1 generated from a designed human synthetic antibody phage library. J. Mol. Biol. 10.1016/j.jmb.2006.11.021, in press.

Liu, W., Parikh, A.A., Stoeltzing, O., Fan, F., McCarty, M.F., Wey, J., Hicklin, D.J., and Ellis, L.M. (2005). Upregulation of neuropilin-1 by basic fibroblast growth factor enhances vascular smooth muscle cell migration in response to VEGF. Cytokine *32*, 206–212.

Miao, H.Q., Soker, S., Feiner, L., Alonso, J.L., Raper, J.A., and Klagsbrun, M. (1999). Neuropilin-1 mediates collapsin-1/semaphorin III inhibition of endothelial cell motility: Functional competition of collapsin-1 and vascular endothelial growth factor-165. J. Cell Biol. *146*, 233–242.

Miao, H.Q., Lee, P., Lin, H., Soker, S., and Klagsbrun, M. (2000). Neuropilin-1 expression by tumor cells promotes tumor angiogenesis and progression. FASEB J. *14*, 2532–2539.

Murga, M., Fernandez-Capetillo, O., and Tosato, G. (2005). Neuropilin-1 regulates attachment in human endothelial cells independently of vascular endothelial growth factor receptor-2. Blood. *105*, 1992–1999. Published online November 2, 2004. 10.1182/blood-2004-07-2598.

Nakatsu, M.N., Sainson, R.C., Aoto, J.N., Taylor, K.L., Aitkenhead, M., Perez-del-Pulgar, S., Carpenter, P.M., and Hughes, C.C. (2003). Angiogenic sprouting and capillary lumen formation modeled by human umbilical vein endothelial cells (HUVEC) in fibrin gels: The role of fibroblasts and Angiopoietin-1. Microvasc. Res. *66*, 102–112.

Rousseau, S., Houle, F., Landry, J., and Huot, J. (1997). p38 MAP kinase activation by vascular endothelial growth factor mediates actin reorganization and cell migration in human endothelial cells. Oncogene *15*, 2169–2177.

Serini, G., Valdembri, D., Zanivan, S., Morterra, G., Burkhardt, C., Caccavari, F., Zammataro, L., Primo, L., Tamagnone, L., Logan, M., et al. (2003). Class 3 semaphorins control vascular morphogenesis by inhibiting integrin function. Nature *424*, 391–397.

Six, I., Kureishi, Y., Luo, Z., and Walsh, K. (2002). Akt signaling mediates VEGF/VPF vascular permeability in vivo. FEBS Lett. *532*, 67–69.

Soker, S., Takashima, S., Miao, H.Q., Neufeld, G., and Klagsbrun, M. (1998). Neuropilin-1 is expressed by endothelial and tumor cells as an isoform-specific receptor for vascular endothelial growth factor. Cell *92*, 735–745.

Soker, S., Miao, H.Q., Nomi, M., Takashima, S., and Klagsbrun, M. (2002). VEGF165 mediates formation of complexes containing VEGFR-2 and neuropilin-1 that enhance VEGF165-receptor binding. J. Cell. Biochem. *85*, 357–368.

Takahashi, T., Ueno, H., and Shibuya, M. (1999). VEGF activates protein kinase C-dependent, but Ras-independent Raf-MEK-MAP kinase pathway for DNA synthesis in primary endothelial cells. Oncogene *18*, 2221–2230.

Takahashi, T., Yamaguchi, S., Chida, K., and Shibuya, M. (2001). A single autophosphorylation site on KDR/Flk-1 is essential for VEGF-A-dependent activation of PLC-gamma and DNA synthesis in vascular endothelial cells. EMBO J. *20*, 2768–2778.

Takashima, S., Kitakaze, M., Asakura, M., Asanuma, H., Sanada, S., Tashiro, F., Niwa, H., Miyazaki Ji, J., Hirota, S., Kitamura, Y., et al. (2002). Targeting of both mouse neuropilin-1 and neuropilin-2 genes severely impairs developmental yolk sac and embryonic angiogenesis. Proc. Natl. Acad. Sci. USA *99*, 3657–3662.

Vanveldhuizen, P.J., Zulfiqar, M., Banerjee, S., Cherian, R., Saxena, N.K., Rabe, A., Thrasher, J.B., and Banerjee, S.K. (2003). Differential expression of neuropilin-1 in malignant and benign prostatic stromal tissue. Oncol. Rep. *10*, 1067–1071.

Wang, L., Zeng, H., Wang, P., Soker, S., and Mukhopadhyay, D. (2003). Neuropilin-1-mediated vascular permeability factor/vascular endothelial growth factor-dependent endothelial cell migration. J. Biol. Chem. *278*, 48848–48860.

Wang, L., Mukhopadhyay, D., and Xu, X. (2006). C terminus of RGS-GAIP-interacting protein conveys neuropilin-1-mediated signaling during angiogenesis. FASEB J. *20*, 1513–1515.

Wey, J.S., Gray, M.J., Fan, F., Belcheva, A., McCarty, M.F., Stoeltzing, O., Somcio, R., Liu, W., Evans, D.B., Klagsbrun, M., et al. (2005). Overexpression of neuropilin-1 promotes constitutive MAPK signalling and chemoresistance in pancreatic cancer cells. Br. J. Cancer *93*, 233–241.

Yuan, L., Moyon, D., Pardanaud, L., Breant, C., Karkkainen, M.J., Alitalo, K., and Eichmann, A. (2002). Abnormal lymphatic vessel development in neuropilin 2 mutant mice. Development *129*, 4797–4806.